Visualization in Medicine and Life Sciences (2013)
L. Linsen, H. -C. Hege, and B. Hamann (Editors)

Improving Electrical Impedance Tomography Imaging of the Lung with Patient-specific 3D Models

P. Salz[1], A. Reske[2], H. Wrigge[2], G. Scheuermann[3], H. Hagen[1]

[1] Computer Graphics & HCI Group, University of Kaiserslautern, Germany
[2] Clinic and Policlinic for Anesthesiology and Intensive Care Medicine, University Hospital Leipzig, Germany
[3] Institute for Computer Science, University of Leipzig, Germany

Abstract

Electrical Impedance Tomography (EIT) visualizes conductivity changes inside the thorax, which correlate with breathing and cardiac activity. While featuring high temporal resolution, no patient risks and bedside application, EIT has a very low spatial resolution, and its anatomical correspondence depends crucially on the choice of body model for image reconstruction. In contrast to the state of the art simplified or averaged 2D body models, we propose a workflow to generate patient-specific 3D models from Computed Tomography (CT) segmentations. This method acknowledges the 3D characteristics of EIT-induced currents in the body, while measurements are only performed in 2D. The workflow was designed in collaboration with medical experts such that its applicability in the clinical context becomes feasible. This is in contrast to most other works that only consider isolated algorithms and neglect the clinical demands and tasks. Our approach generates CT segmentations using another novel workflow based on interactive sketching, computes a tetrahedral multi-material mesh and creates a forward model with these results. The GREIT reconstruction algorithm is used to generate EIT images using the 3D model, while its parameters are tuned to the 3D properties of the mesh. We present results from two pigs, with three EIT datasets each, including mechanical ventilation, ventilation under the influence of lung injury, and ventilation-free regional perfusion analysis. We discovered three anatomical phenomena in the improved EIT images that could be visualized and explained using our workflow, while they caused some confusion in image interpretation using the state of the art techniques. These results, though not yet quantitatively measured, show the improved image quality and better anatomical significance, and stress the importance of accurate body models for EIT application in clinical research and patient treatment.

1. Introduction

EIT is a promising imaging technology to visualize conductivity changes in the body. These have been shown to correlate with lung ventilation, regional lung perfusion and cardiac activity. For patients with severe lung injury, this method has the potential to diagnose, observe and evaluate lung damages before, during and after medical treatment. The main advantages of EIT are its high temporal resolution (currently up to 50 images per second), lack of ionizing radiation, inexpensive devices and usage and application at bedside. Most EIT images are functional without direct information about anatomical structures such as the lung boundary. They suffer from low spatial resolution (currently up to 64x64 pixels), severe artifacts and noise, and image quality depends crucially on the model.

EIT imaging is an inverse problem, where conductivity changes inside the body affect voltage measurements on the body surface. A forward model is used to compute the reconstruction matrix that maps a set of measurements to image pixels, taking into account the body geometry, electrodes, known conductivity priors, and other factors. This forward model consists of a Finite Element Mesh with certain conductivity values for each element and other properties. Once the reconstruction matrix for this setup is known, EIT images can be generated using an inverse model that is usually very simplified (i.e. 2D and homogeneous). Instead of absolute conductivity measurements, most medical applications use differential measurements with respect to a baseline, which remedies some of the severe problems that are caused by inaccurate body models. Therefore, EIT image

DOI: 10.2312/PE.VMLS.VMLS2013.049-053

resolution is mostly limited to about 20% of the thorax diameter [AAB*09].

Related Work

While a 2D circular and homogeneous body model was used for a long time, the Dräger PulmoVista 500 device features a forward model generated from a variety of human lung data, and a 2D elliptical inverse model for image reconstruction [TI11]. Ferrario et al. present a quantitative assessment of lung overlap between 2D CT data and EIT images from their 2.5D extruded forward model [FGA*12], which is considered state of the art. These models are easy to generate since only the segmentation of a single CT slice is needed, but they suffer from over- or under-segmentation of the lung and heart, depending on the vertical placement of the electrode plane. Also, true organ shapes are not precisely covered since their appearance is usually not vertically homogeneous.

Fan and Wang use a 3D forward model, but they do not present a practically relevant method of generating them [FW10]. Moreover, they do not show results from EIT data, but merely simulations on the forward model. In contrast, Yang et al. demonstrate a very sophisticated 3D forward model generated from an MRI scan [YZP13]. While this precise model is useful for impedance simulations, its significance for a patient-oriented workflow in the clinical context is quite limited. This is due to the very large number of different materials, the manual segmentation of the MRI data (which takes many hours or days), and the unclear generation of a tetrahedral mesh.

Large efforts are taken in clinical research to study the usefulness of EIT in medical treatment, especially monitoring lung recruitment maneuvers, deducing quantitative characteristics from EIT data, and comparison to CT images [WZM*08, RRH*11, MLZ*12].

Finally, the EIDORS framework [AL06] and the included Graz concensus EIT reconstruction algorithm GREIT [AAB*09] provide a very good base for EIT experiments and are therefore used and extended in our work. GREIT is a novel approach to EIT imaging since it optimizes the reconstruction matrix regarding several figures of merit using virtual conductivity targets that are placed inside the forward model.

Data

Our medical collaborators provided two pig datasets, containing CT and EIT data. The CT scans have an in-plane resolution of about 0.6 mm and a vertical resolution of 5 mm. They also show the 16 electrodes attached to the thorax, which is not common in medical treatment, but suitable for animal studies.

The EIT data is recorded with the Dräger PulmoVista 500 mentioned above, at a temporal resolution of 20 Hz for the first pig, and 50 Hz for the second pig. We have data available before and after application of lung damage, as well as a dataset featuring apnea and injection of a saline bolus in the blood flow to study regional lung perfusion.

2. Method

The EIT community agrees that a patient-specific 3D model would be very useful, but is considered difficult to generate [AAB*09, AAA*12]. Also, availability of patient data is an important issue. Our workflow starts with the segmentation of a CT scan of the patient, which is acquired in clinical routine. A 3D tetrahedral mesh is generated from the segmentation and converted to a forward model. The most important contribution of our workflow is its focus on the clinical context. It was designed in collaboration with medical experts and always keeps the applicability for medical research and clinical tasks in mind.

CT Segmentation

Our semi-automatic segmentation workflow (presented by Salz et al. [SRW*12] and submitted for publication) uses the medical expert's knowledge about the lung shape and other anatomical properties in an interactive and fast way. Its central element is the sketch-based selection of pathological lung tissue. It is much faster than the state of the art (manual contouring), and has the potential to be used in practice, in contrast to most other algorithms, which are quite isolated and not ready for clinical application.

The output of this step is a set of 3D masks for the different materials of interest, namely thorax shape, lung, heart, and electrode locations.

3D Model Generation

We first reconstruct the electrode shapes from the positions and known dimensions such that they touch the thorax in each slice. This step is necessary because the electrodes cannot be segmented from the CT data directly due to partial volume effects and other metal-induced artifacts. From the segmentation we generate a multi-material tetrahedral mesh using BioMesh 3D [SCI]. This includes a tightening step to smooth boundaries and a particle-based seed point placement on material junctions. The particles are distributed along the boundaries by an advection process and serve as input for the meshing process. The meshing is done with a Delaunay tetrahedralization. The output of this step is a mesh with about 500000 elements and 250000 vertices, which is a moderate mesh size, while maintaining very high mesh quality and adaptivity.

To comply with the EIDORS specification for forward models, we compute the boundary surface of the thorax and contact surfaces of the electrodes and the boundary. To find

the correct ordering of the electrodes, we project the electrode vertices in the electrode plane and use a kernel density estimation to get their centroids. These are used as seed points for a k-means clustering (with $k = 16$). Each electrode vertex now has the corresponding cluster (i.e. electrode) number, which can be assigned to the 3D vertex. The ordering is then done by sorting the polar angles of the electrodes.

EIT Image Reconstruction

The GREIT reconstruction algorithm is designed to work with 3D meshes. The reconstruction matrix is computed by training conductivity targets inside the mesh according to the GREIT specifications. With a forward simulation of this setup and an intermediate image reconstruction, GREIT optimizes certain figures of merit which results in very good EIT images. According to the specifications, targets are distributed randomly and are vertically displaced with an offset of up to 25% of the thorax diameter. A mapping from the 3D mesh to the 2D inverse model is computed automatically by EIDORS.

3. Results

Three EIT datasets are used for each of the two pigs: The first features mechanical ventilation without lung damage. The second is recorded after application of the lung damage (which affects mostly dorsal tissue due to gravity), so some of the lung tissue is non-ventilated or collapsed. The last dataset is from a state of apnea with injection of a saline bolus in the blood flow to study regional lung perfusion.

CT Visualization

The CT data indicates a low electrode placement in one pig, so we should expect the EIT images to show more activity of the lower lung and less cardiac activity. Moreover, the 2.5D extruded models (see below) suffer from an oversegmented lung shape because the heart is quite small in the respective CT slice.

As an indicator of lung overlap between EIT and CT data we mimic the EIT characteristics by projecting the CT segmentation into the electrode plane (in contrast to Ferrario et al. who use the respective CT slice [FGA*12]). Each slice is weighted with decreasing weights for increasing distance to the plane. A color-coding for the red, green and blue channels is done for the lung, non-lung and electrode materials. Note that for the perfusion dataset, we changed the color-coding due to a different color map in the EIT data. The lung shape in the CT projection is extracted by thresholding all pixels that feature a contribution of the lung of more than two thirds. EIT images are resized and interpolated to match the much larger CT image resolution (512x512 compared to 64x64 pixels).

EIT Models

The 3D model is cropped around an offset of 30% of the thorax diameter above and below the electrode plane to remove barely contributing regions. To compare our method to the state of the art we generated two 2.5D models by extruding a single slice segmentation, one without and one with explicit lung shape. The first model is used by Ferrario et al. [FGA*12], while the second is available in the EIDORS package. For the second 2.5D model and the 3D model a different conductivity prior value for the lung than for the thorax was used. For comparison, we put the real size EIT image in the top left of each image to show the large difference in resolution.

Fig. 1 and Fig. 2 show our results for two pigs. In the top row, an overview of the data is given, with a visualization of the thorax mesh on the left, a projection of the CT segmentation into the electrode plane with highlighted lung shape in the middle, and a sample EIT timestep on the right. The other rows show the different EIT datasets. The images in the left column are from the 2.5D approach without lung shape consideration. The middle column shows results from the 2.5D model with lung shape, and the right column shows our results using the proposed individualized 3D model with lung shape and electrode positions.

4. Discussion

We observed that our EIT images show a better overlap with the real lung shape in the projected CT image compared to the 2.5D models. There is no general consensus on how to quantitatively assess EIT image quality, but Ferrario et al. [FGA*12] propose to compute this overlap, which we will do in the future. Instead we demonstrate how our EIT images revealed three important phenomena that can cause confusion during image interpretation.

From the 3D model of the first pig (Fig. 1a) we noticed that the electrode belt was placed slightly tilted. Since the 2.5D models (Fig. 1b left and middle) assume a symmetric placement of the electrodes, the images feature an asymmetry that is directly related to the belt shift. Our model considers the exact electrode locations, and therefore the EIT images show the healthy and symmetric lung, as expected (Fig. 1b right).

In the second pig dataset (see Fig. 2b) we note a lower lung boundary in the dorsal area of one lung. A comparison with the CT data reveals that this pig has some non-ventilated lung tissue on this side of the lower lung, and since we know that the electrode belt is placed lower than usual, we expect the EIT images to show more activity of the lower lung. Without this knowledge, one might relate this asymmetry to the aforementioned electrode belt shift.

The results using our model for the dataset featuring cardiac and perfusion activity of the second pig not only show

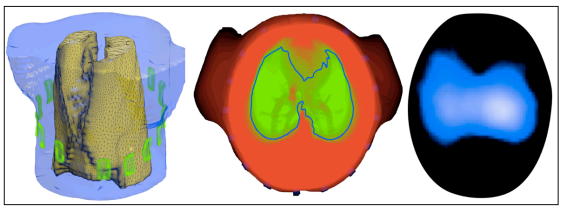

(a) Data overview for the first pig.

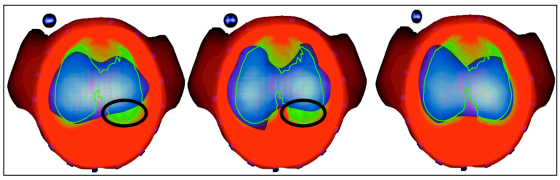

(b) No lung damage. The circled regions show an artifact caused by an electrode belt shift.

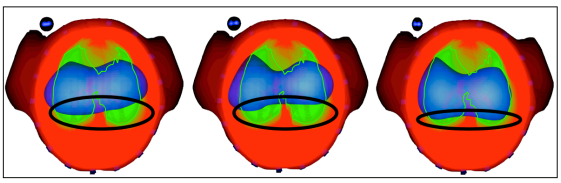

(c) With lung damage (circled regions).

Figure 1: Results for the first pig dataset. Left: From 2.5D model without lung. Middle: 2.5D with lung. Right: From our 3D model.

a better correspondence to how the regional blood flow projected into the electrode plane would look like, but the saline bolus was also applied during a state of lung injury in the dorsal region (Fig. 2d). As the circled region in our image reveals, it seems that some of the dorsal lung tissue is not only non-aerated, but also non-perfused. This is a very important characteristic for regional lung perfusion analysis and further investigations will be done in the future to confirm this finding.

5. Conclusion

We presented a workflow to construct individualized 3D forward models for EIT image reconstruction, based on the availability of a CT segmentation approach. We showed EIT images from the 3D model and compared them visually to the 2.5D state of the art models. We visually noted a moderate increase in image quality, while we could discover and explain three anatomical phenomena (electrode belt shift, prior lung injury, non-perfused lung tissue), which was not possible before. In fact, these phenomena caused a notable confusion when interpreting the state of the art images. We are confident that our workflow is useful for assessing the lung boundary and non-ventilated lung tissue from EIT images before and after medical treatment.

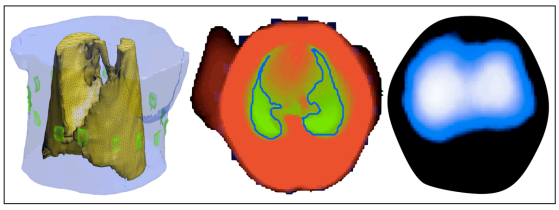

(a) Data overview for the second pig.

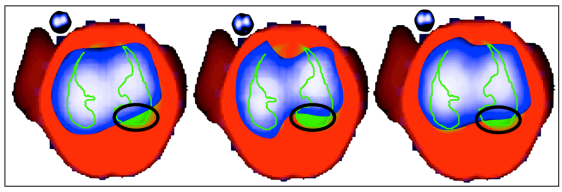

(b) With prior lung damage (circled region).

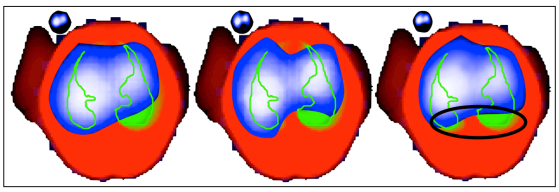

(c) With additional lung damage. The circled region shows how our method reveals this injury properly.

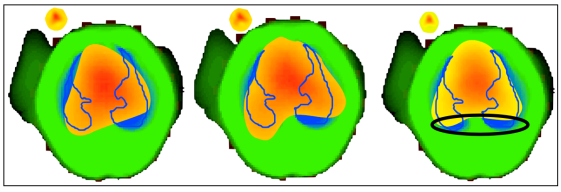

(d) Apnea and perfusion. The circled region shows (probably) non-perfused, non-aerated lung tissue.

Figure 2: Results for the second pig dataset. Left: From 2.5D model without lung. Middle: 2.5D with lung. Right: From our 3D model.

6. Future Work

Our next steps include the explicit modeling of the heart and pathological lung tissue in the 3D model. These structures are already available form the segmentation. We also plan to perform the quantitative assessment of the overlap of CT and EIT lung shape as done by Ferrario et al. [FGA*12]. Finally, we have much more pig data available to conduct a large comparison study and we also plan to test our approach on human EIT data.

References

[AAA*12] ADLER A., AMATO M. B., ARNOLD J. H., BAYFORD R., BODENSTEIN M., BÖHM S. H., BROWN B. H., FRERICHS I., STENQVIST O., WEILER N., WOLF G. K.: Whither lung EIT: Where are we, where do we want to go, and what do we need to get there? *Physiol. Meas. 33* (2012), 679–694. 2

[AAB*09] ADLER A., ARNOLD J. H., BAYFORD R., BORSIC A., BROWN B. H., DIXON P., FAES T., FRERICHS I., GAGNON H., GÄRBER Y., OTHERS: GREIT: a unified approach to 2D linear EIT reconstruction of lung images. *Physiol. Meas. 30* (2009), S35. 2

[AL06] ADLER A., LIONHEART W. R. B.: Uses and abuses of EIDORS: an extensible software base for EIT. *Physiol. Meas. 27*, 5 (2006), S25–42. 2

[FGA*12] FERRARIO D., GRYCHTOL B., ADLER A., SOLA J., BOHM S., BODENSTEIN M.: Toward Morphological Thoracic EIT: Major Signal Sources Correspond to Respective Organ Locations in CT. *IEEE Transactions on Biomedical Engineering 59*, 11 (2012). 2, 3, 4

[FW10] FAN W. R., WANG H. X.: 3D modelling of the human thorax for ventilation distribution measured through electrical impedance tomography. *Measurement Science and Technology 21*, 11 (2010). 2

[MLZ*12] MUDERS T., LUEPSCHEN H., ZINSERLING J., GRESCHUS S., FIMMERS R., GUENTHER U., BUCHWALD M., GRIGUTSCH D., LEONHARDT S., PUTENSEN C., WRIGGE H.: Tidal recruitment assessed by electrical impedance tomography and computed tomography in a porcine model of lung injury. *Crit. Care Med 40*, 3 (2012), 903–11. 2

[RRH*11] RESKE A. W., RESKE A. P., HEINE T., SPIETH P. M., RAU A., SEIWERTS M., BUSSE H., GOTTSCHALDT U., SCHREITER D., BORN S., ET AL.: Computed tomographic assessment of lung weights in trauma patients with early posttraumatic lung dysfunction. *Crit. Care Med. 15*, 1 (2011), S71. 2

[SCI] BioMesh3D: Quality Mesh Generator for Biomedical Applications. Scientific Computing and Imaging Institute (SCI). URL: http://www.biomesh3d.org. 2

[SRW*12] SALZ P., RESKE A., WRIGGE H., SCHEUERMANN G., HAGEN H.: User-guided Segmentation of Thoracic Computed Tomography Data for Electrical Impedance Tomography Image Reconstruction. *Poster at the BioVis symposium* (2012). 2

[TI11] TESCHNER E., IMHOFF M.: *Electrical Impedance Tomography: The realization of regional ventilation monitoring*. Tech. rep., 2011. 2

[WZM*08] WRIGGE H., ZINSERLING J., MUDERS T., VARELMANN D., GÜNTHER U., VON DER GROEBEN C., MAGNUSSON A., HEDENSTIERNA G., PUTENSEN C.: Electrical impedance tomography compared with thoracic computed tomography during a slow inflation maneuver in experimental models of lung injury. *Crit. Care Med. 36*, 3 (2008), 903–9. 2

[YZP13] YANG F., ZHANG J., PATTERSON R.: Development of an Anatomically Realistic Forward Solver for Thoracic Electrical Impedance Tomography. *Journal of Medical Engineering* (2013). 2